PCCP

PAPER

View Article Online
View Journal | View Issue

Cite this: *Phys. Chem. Chem. Phys.*, 2025, **27**, 9068

Accurate prediction of ionic liquid density-of-states from low-cost calculations†

Richard M. Fogarty, [a] Richard P. Matthews, [ab] Patricia A. Hunt *[ac] and Kevin R. J. Lovelock *[d]

Received 16th January 2025,
Accepted 19th March 2025

DOI: 10.1039/d5cp00214a

rsc.li/pccp

The electronic structure of ionic liquids (ILs) is a key factor in their chemical reactivity. Experimental techniques provide insight into IL electronic structure (*e.g.*, X-ray photoelectron spectroscopy, XPS), but are impractical for screening large numbers of potential ILs. Computational screening offers an alternative approach, but current *ab initio* calculation methods (ion-pairs or large calculations with periodic boundaries) are not suitable for screening. We establish that a simple and computationally low-cost method, lone-ions evaluated at the B3LYP-D3(BJ)/6-311+G(d,p) level employing a generalised solvation model SMD (solvation model based on density), captures IL liquid-phase density-of-states (DoS) with good accuracy by validating against XPS data for a wide range of ILs. The additivity of the results from individual lone-ion calculations provides a significant advantage, enabling predictions of the DoS for a large number of ILs and delivering a significant step towards the computational screening of ILs for many applications.

Introduction

Ionic liquids (ILs) have the potential to impact on a broad range of technologies where knowledge of the density of states (DoS)[1–3] is critical: electrochemical applications (supercapacitors, fuel cells, photoelectrochemical cells, batteries),[4–7] photochemical applications,[6–9] nuclear fuel processing,[10] deconstruction of lignocellulosic biomass,[11] and gas separation/capture/storage.[12,13] Identification of the most reactive states, especially the energy and composition of the highest occupied molecular orbital (HOMO),[14] and measurement of the IL ionisation energy, E_i(IL), are vital for understanding and predicting any process/property underpinned by electron donation, *e.g.*, electrochemical oxidative stability[15–17] to give better supercapacitors,[18] thermal stability, IL basicity, or supporting/participating in chemical reactions.[19,20] For traditional salts such as NaCl HOMO identification is easy; the anion highest occupied fragment orbital (HOFO) is always the HOMO. In contrast, for ILs the larger and chemically more complex ions often make HOMO identification challenging; for a small but significant proportion of ILs (counter-intuitively) the cation HOFO is the HOMO.[21–23]

The possibility, out of the potentially vast number of ILs, that an ideal IL exists for a particular application is an appealing prospect. The challenge is to identify the optimal IL. Large-scale experimental screening is daunting, making computational screening hugely advantageous. The use of expensive and technically demanding *ab initio* methods or DFT molecular dynamics to provide reliable computational results is well established for ILs.[24] Computational methodologies for screening significant quantities of ILs must avoid such expensive, technically demanding calculations, but still capture sufficient information, in particular the solvation environment of the cations and anions, to be representative of the IL. Therefore, critical in the context of large-scale screening is the minimum level of computation required to reliably deliver information on liquid-phase ions.

To have high confidence in the predictions produced by any computational method, experimental validation is essential. The most established validation procedure for the electronic structure of ILs is a visual match of the calculated IL DoS with the experimental valence electronic structure measured using non-resonant valence X-ray photoelectron spectroscopy (XPS, *e.g.*, $h\nu$ = 1486 eV) and/or ultraviolet photoelectron spectroscopy (UPS, *e.g.*, $h\nu$ = 21.2 eV).[25–43] Gelius-weighted IL DoS, where photoionisation cross-sections are included,[44] can give more confidence in the computed spectra.[33–35,37–41] However, the reliance on a purely visual validation of computed spectra with experimental spectra is unsatisfactory and will not work for many ILs, given that anion contributions dominate the experimental photoelectron spectra, meaning that cation contributions cannot be observed and validated.

A more quantitative validation of DoS calculations is now possible using recently reported experimental XPS data for 60

[a] *Department of Chemistry, Imperial College London, UK*
[b] *School of Health, Sport and Bioscience, University of East London, UK*
[c] *School of Chemical and Physical Sciences, Victoria University of Wellington, New Zealand. E-mail: patricia.hunt@vuw.ac.nz*
[d] *Department of Chemistry, University of Reading, UK. E-mail: k.r.j.lovelock@reading.ac.uk*

† Electronic supplementary information (ESI) available. See DOI: https://doi.org/10.1039/d5cp00214a

ILs, which includes values for E_i(IL) and the energy difference between the cation and anion highest occupied orbitals within the IL environment, ΔE_B(ion HOFO) = E_B(cation HOFO) – E_B(anion HOFO) (where E_B = binding energy).[21,22] In particular the comparison of calculated and experimental ΔE_B(HOFO) values allows us to validate the ability of the calculated DoS to the capture liquid-phase ion–ion solvation environment of both the cation and anion.

There is currently no established method of calculating the IL DoS that is inexpensive and technically undemanding. Calculations of ion-pairs in the gas-phase (ion-pair-GP), which are relatively inexpensive but reasonably technically demanding, perform acceptably, although small E_B shifts are required to obtain a good visual match of the IL DoS with experimental valence XP spectra.[30,32–35,37] Summation of individual lone-ions-GP DoS to produce an IL DoS are inexpensive and technically undemanding, but do not adequately capture the bulk IL DoS.[25–29,32,37]

IL DoS can potentially be captured within a liquid environment using a generalised solvation model SMD (solvation model based on density),[45,46] which involves placing the substrate/solute in a cavity and representing the surrounding liquid as a charge distribution on the cavity surface. The SMD model can account for electrostatic effects on electronic structure, but not specific covalent interactions such as ion–ion coordination within the first solvation sphere. Recently, anion–cation interactions in ILs were established to be primarily electrostatic and non-specific using a combination of E_B(core) from XPS and very expensive and technically demanding *ab initio* molecular dynamics calculations.[47] These results indicate that the SMD might work well for IL DoS.

In the current manuscript we report on an efficient and accurate computational method for evaluating IL DoS. The methodology is validated against a range of experimental data and more complex calculations. Two new quantitative (non-visual) validation methods are presented, using recently published E_i(IL) and ΔE_B(ion HOFO) experimental data for 39 ILs[21,22] to establish the accuracy of the computed IL DoS (Fig. 1c and d). The validated method is then applied to a wide range of IL systems, demonstrating the ability to screen and provide predictive information for 560 ILs (Fig. 2). The ions studied cover a wide chemical space, including six imidazolium cations, a phosphonium cation, two ammonium cations, and 35 anions; see ESI,† Section S1 for a full list including chemical structures.

Methodology

DFT calculations were carried out at the B3LYP-D3(BJ) level, using Becke's three-parameter exchange functional in combination with the Lee, Yang and Parr correlation functional (B3LYP) as implemented in the Gaussian 09 and Gaussian 16 suites of programs.[48–51] Grimme's D3 dispersion correction with Becke–Johnson damping was used to account for dispersion.[52–55] The 6-311+G(d,p) basis set was employed for lighter atoms (H, C, N, O, F, Al, P, S, Cl, Fe, Co, Ni, Cu, Zn, Ga), except for calculations undertaken to test the effects of varying the basis set which are discussed further below.[56–59] LANL2DZdp pseudo potentials and the associated basis sets were employed for the heavier atoms Br, Sn, Sb, I; the LANL2DZ pseudo potential and the associated basis sets was employed for the heavier atom In.[60] For the $[Bi_2Cl_8]^{2-}$ anion, data was taken from calculations included in ref. 61 cc-pVDZ-pp (scalar relativistic) pseudopotentials and aug-cc-pVDZ associated basis sets were employed for the heavy Bi atom,[62,63] and the aug-cc-pVDZ basis set was employed for Cl.

Optimisation was carried out without symmetry constraints. The SCF convergence criteria were tightened from the Gaussian 09 defaults to 10^{-9} on the density matrix and 10^{-7} on the energy matrix (scf = conver = 9). The numerical integration grid was a pruned grid with 99 radial shells and 590 angular points per shell (int = ultrafine). Frequency analysis was carried out for all optimised structures, which are confirmed as minima by the absence of imaginary modes.

The SMD (solvation model based on density) was used.[46] Unless otherwise stated, $[C_4C_1Im][SCN]$ SMD parameters were used for $[C_4C_1Im][SCN]$ IL calculations while $[C_4C_1Im][PF_6]$ parameters were used for calculations for other ILs (very slightly different SMD parameters were used for the $[Bi_2Cl_8]^{2-}$ anion as detailed in ref. 61 and 64). Some testing of the relative permittivity (ε_r) was carried out using default parameters within G09 and G16. The SMD parameters employed are shown in Table S3 (ESI†).

Gelius-weighted IL DoS were computed (lone-ions-GP, lone-ions-SMD, ion-pair-GP, ion-pair-SMD, dimer-GP and dimer-SMD, where dimer = two ion-pairs); for lone-ions-SMD the IL DoS was produced *via* summation of individual cation and anion lone-ion-SMD DoS. A single E_B shift is applied to align the computed HOMO (lowest E_B, *i.e.*, right most peak in Fig. 1a and b) of the DoS with the lowest E_B XPS peak.

Further computational details can be found in the ESI,† Section S2.

Results and discussion

Excellent visual (*i.e.* qualitative) matches of both cation and anion components are obtained between non-resonant valence XP spectra and calculated DoS using the lone-ions-SMD methodology (Fig. 1 and ESI,† Sections S3–S5), which validates the ability of this methodology to recover liquid-phase inter-ion solvation. Specifically, the computed IL DoS is comprehensively validated by the superb visual match to the experimental valence XP spectra for two key ILs, $[C_4C_1Im][SCN]$ ($[C_4C_1Im]^+$ = 1-butyl-3-methylimidazolium, Fig. 1a and Fig. S3, ESI†) and $[C_8C_1Im]Cl$ ($[C_8C_1Im]^+$ = 1-octyl-3-methylimidazolium Fig. S2, ESI†), where both the cation and anion contributions can be easily identified using XPS, especially at low $h\nu$. For $[C_4C_1Im][SCN]$ the red trace of the lone-ions-SMD calculated spectrum and the black trace of the experimental spectrum show an excellent visual match (Fig. 1a). The more expensive model systems (dimer-GP, ion-pair-SMD and dimer-SMD) also perform well overall. The ion-pair-GP DoS (Fig. 1a blue trace) gives an acceptable match but is not quite as good as the lone-ions-SMD (Fig. 1a red trace). For $[C_4C_1Im][SCN]$, all computational methods show that the HOMO is from the anionic HOFO, see the peak at $E_B \sim 7.5$ eV, which is

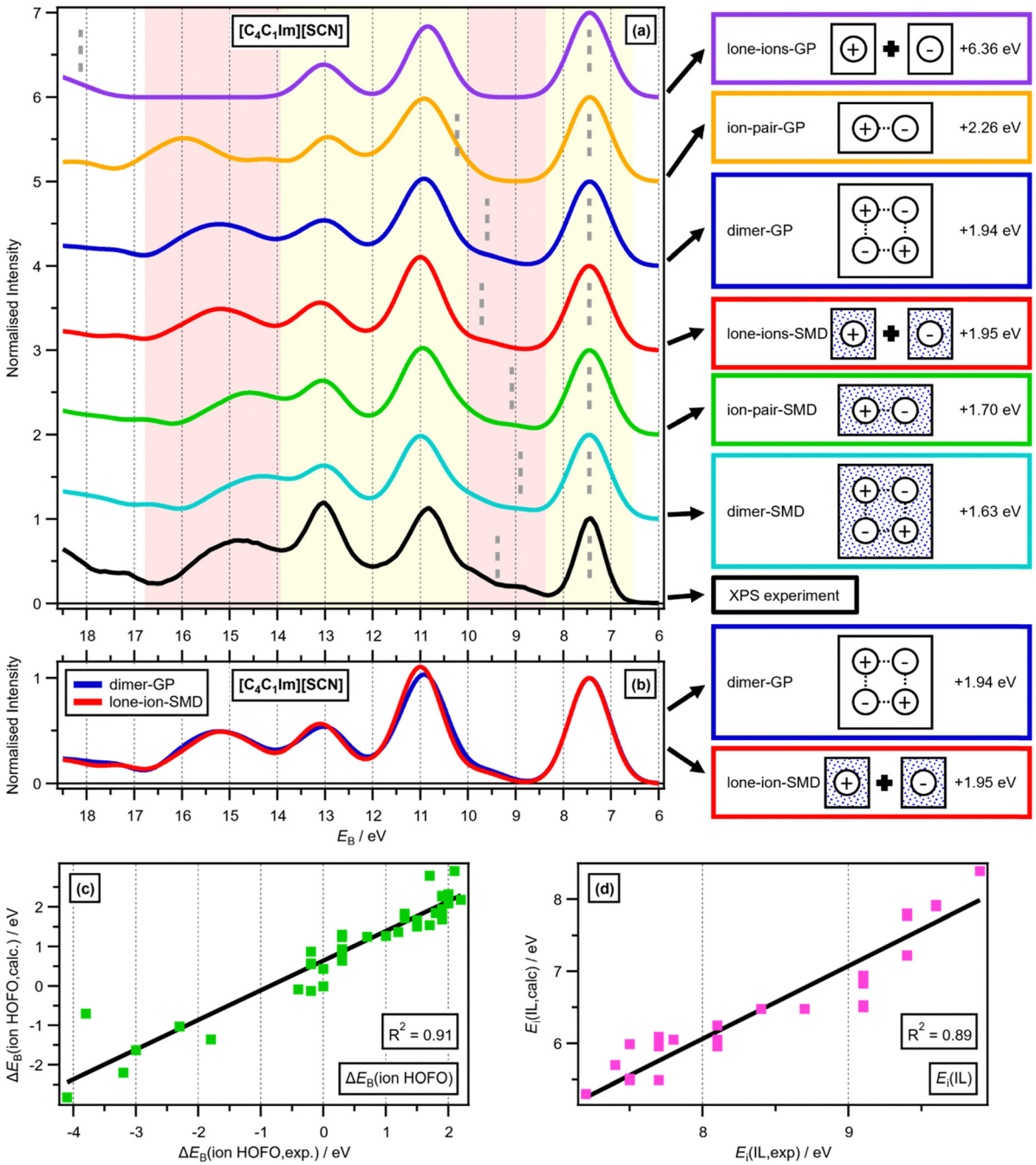

Fig. 1 (a) Comparison of the experimental non-resonant valence XP spectrum (recorded at $h\nu$ = 161.0 eV) with calculated Gelius-weighted DoS (calculated at $h\nu$ = 160 eV) for varying model systems for $[C_4C_1Im][SCN]$, vertically offset for clarity. The yellow and pink filled rectangles are to guide the eye to the E_B regions where anionic and cationic contributions respectively dominated the experimental valence XP spectrum. The vertical dashed grey lines represent the calculated cation HOFO energies and anion HOFO energies for the different systems, demonstrating ΔE_B(ion HOFO) for each system. The experimental valence XP spectrum was charge corrected as given in ref. 22. (b) Comparison of calculated Gelius-weighted DoS (calculated at $h\nu$ = 160 eV) for two model systems (dimer-GP and lone-ions-SMD) for $[C_4C_1Im][SCN]$. A single shift was applied to each of the calculated Gelius-weighted DoS; the E_B shift value for each calculated Gelius-weighted DoS is given on the extreme right-hand side of the figure. Correlations of experimental (taken from ref. 22) and calculated descriptors of IL electronic structure: (c) ΔE_B(ion HOFO) and (d) ionisation energy, E_i(IL). Calculations are for lone-ions-SMD (39 ILs in total).

consistent with experimental results.[21] A low intensity but crucial feature is the "bump" at $E_B \sim 9$ eV (black trace), due to the $[C_4C_1Im]^+$ cation HOFO, which is present in the lone-ions-SMD DoS (red trace) at $E_B \sim 9.5$ eV (marked by a vertical dashed grey line). Moreover, the lone-ions-SMD DoS gives an excellent match to the experimental spectrum for the peaks due to cationic MOs at $E_B \sim 15$ eV (important, given that the E_B shift was made with respect to the anion HOFO).

Further validation of the ability of the lone-ions-SMD methodology to recover the liquid-phase inter-ion solvation is

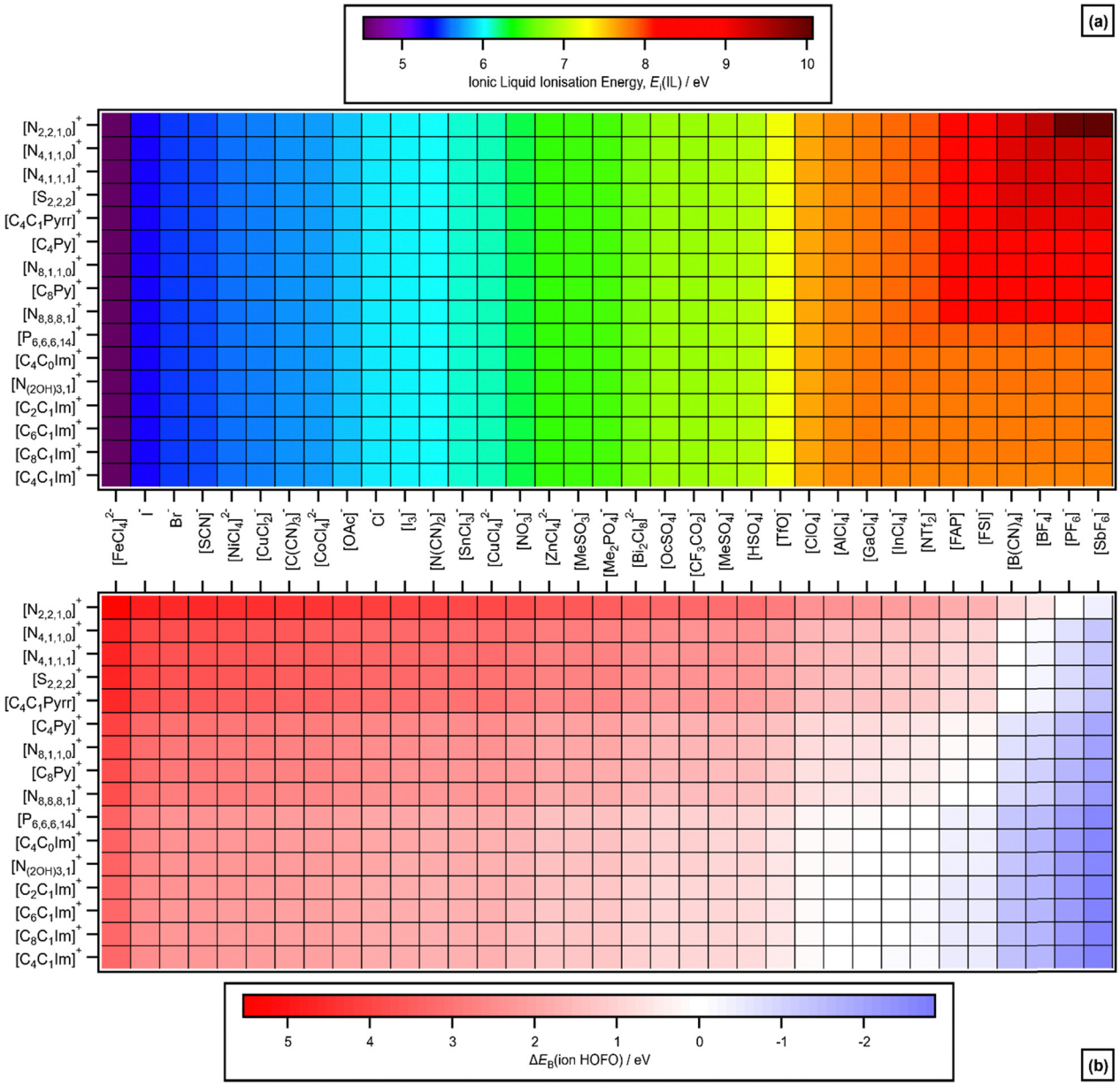

Fig. 2 Predictions using lone-ions-SMD. (a) IL ionisation energies, E_i(IL,calc.) for lone-ions-SMD. (b) ΔE_B(ion HOFO,calc.) = E_B(cation HOFO,calc.) – E_B(anion HOFO,calc.) for lone-ions-SMD. When ΔE_B(ion HOFO,calc.) is positive the anion is the IL HOMO (red), when ΔE_B(ion HOFO,calc.) is negative the cation is the IL HOMO (blue) and when ΔE_B(ion HOFO,calc.) is zero either the cation and the anion could be the IL HOMO (white). E_i(IL,calc.) for lone-ions-SMD used to produce these graphs are given in ESI,† Tables S12 and S13.

evidenced by excellent visual matches of calculated DoS and three different experimental XPS data types. First, good visual matches are obtained at different $h\nu$ for lone-ions-SMD DoS and experimental valence XPS for both $[C_4C_1Im][SCN]$ and $[C_8C_1Im]Cl$ (ESI,† Fig. S2 and S3); the relative peak areas of XP spectra vary depending on the wavelength of the light, and the use of Gelius-weighting allows this variation to be recovered by the lone-ions-SMD DoS calculations. Second, computed lone-ion-SMD DoS show superb visual matches to experimental lone-ion valence XPS data for 12 anions and four cations (ESI,† Section S4), validating the calculations; for example, all four cyano-containing anions give excellent visual matches to the calculated lone-ion DoS to experimental data (ESI,† Fig. S5). Third, computed lone-ion-SMD partial DoS for one atomic orbital show good visual matches to experimental valence resonant XPS data for six anions and five cations (ESI,† Section S5), again validating the calculations; for example, for $[HSO_4]^-$ the O 2p lone-ion-SMD partial DoS visually matches very well to the experimental oxygen valence resonant XPS data (ESI,† Fig. S8f).

Quantitative comparisons using two different parameters/metrics show that the lone-ions-SMD method recovers the liquid-phase inter-ion solvation very well. First, the quantitative comparison of ΔE_B(ion HOFO,exp.)[22] *versus* ΔE_B(ion HOFO,lone-ions-SMD) gives an excellent linear correlation (R^2 = 0.91, Fig. 1c).

For example, for $[C_4C_1Im][SCN]$ lone-ions-SMD gave ΔE_B(ion HOFO,calc.) = 2.2 eV, which is the same (within error limits) as ΔE_B(ion HOFO,exp.) = 1.9 eV ± 0.5 eV.[21] In contrast, ΔE_B(ion HOFO,lone-ions-GP) gives a poor linear correlation (R^2 = 0.36, ESI,† Fig. S10a).

In the second quantitative assessment, comparison of E_i(exp.) taken from ref. 22 with E_i(calc.) (*i.e.*, the calculated HOMO E_B) for lone-ions-SMD gives a good linear correlation with R^2 = 0.89 (Fig. 1d). In contrast, E_i(lone-ions-GP) gives a poor correlation with R^2 = 0.50 (ESI,† Fig. S11a). These results also show that lone-ions-SMD calculations are sufficient to capture the relative difference in E_i between different ions. The *y*-intercept = −2.2 eV of Fig. 1d does not go through zero demonstrating an approximately constant error relative to E_i(exp.). For $[C_4C_1Im][SCN]$, E_i(dimer-SMD), which is expected to give accurate results, is 1.63 eV lower than E_i(exp.). This result suggests that both the approximately constant offset between E_i(calc.) and E_i(exp.) and the need for a single E_B shift to align computed HOMO (top of the DoS) with the lowest E_B XPS peak is due to the DFT method, rather than the SMD method not capturing the liquid-phase solvation environment.[65–67] Our results are consistent with previous studies where strong linear correlations (but with non-zero intercepts) were observed between DFT and experimental E_i for a wide range of functionals and molecules.[68,69]

Our calculations appear to have picked up a flaw in the experimental analysis for one IL, demonstrating that calculations can provide a valuable check for experimental results. An outlier for the correlation in ΔE_B(ion HOFO) is the IL $[C_2C_1Im][FAP]$ ($[C_2C_1Im]^+$ = 1-ethyl-3-methylimidazolium and $[FAP]^-$ = tris(pentafluoroethyl)trifluorophosphate), ΔE_B(ion HOFO,lone-ions-SMD) = −0.70 eV compared to ΔE_B(ion HOFO,exp.) = −3.8 eV (Fig. 1c). On close inspection of the experimental results published in ref. 22 we expect that there was a small anion contribution at a similar E_B to the cation contribution, which was very challenging to observe experimentally due to the overlap of the cationic and anionic experimental contributions, leading to an incorrect assignment of the anion E_B(HOFO).

Lone-ions-SMD captures the liquid-phase solvation for dianion-containing ILs very well. Two of the ILs studied contained dianions, $[P_{6,6,6,14}]_2[ZnCl_4]$ ($[P_{6,6,6,14}]^+$ = tetradecyl(trihexyl)phosphonium) and $[C_8C_1Im]_2[ZnCl_4]$. These results provide evidence that no special treatment (beyond lone-ions-SMD) is required for ILs containing dianions.

A sum of non-specific electrostatic inter-ion interactions, as present in lone-ions-SMD, have the same effect on IL orbital energies as found in an explicit larger cluster, *i.e.*, a dimer. Knowledge of the relative impact of generalised, non-specific solvent interactions, *versus* specific (covalent or ionic) ion-pair interactions is highly desirable. For $[C_4C_1Im][SCN]$ the computed DoS for the dimer-GP and sum of lone-ions-SMD are visually near identical (Fig. 1b). Moreover, the individual ion E_i(HOFO) and in the IL E_i(HOMO) shift required to visually match the experimental XP spectrum is near identical, +1.95 eV and +1.94 eV respectively.

For the most important input parameter in the SMD model, the relative permittivity ε_r, ∼11 is a good general value for predictions of screening, with an E_i(HOFO) error of $< \pm 0.2$ eV. For ILs $7.5 < \varepsilon_r < 20$ is the normal range of experimental ε_r values.[70–73] A single value for ε_r that can reasonably represent any IL is highly desirable to simplify the survey procedure. Within the SMD model the dependence of MO energies on ε_r has been evaluated (ESI,† Section S7 and Fig. S12). The impact on ΔE_B(ion HOFO) is shown to scale as $(\varepsilon_r - 1)/\varepsilon_r$ (ESI,† Fig. S13). A simple estimate for the error incurred using a generalised representative ε_r parameter can be determined by comparing the change in lone-ions-SMD E_i(cation HOFO) over a range of ε_r. The change in E_i(cation HOFO) lone-ions-SMD for ε_r = 7.5 to 20, for a dialkylimidazolium cation is 0.4 eV (ESI,† Fig. S13), with the average E_i(cation HOFO, lone-ions-SMD) occurring at $\varepsilon_r \sim 11$.

Based on the results presented thus far, we have established that an excellent compromise between accuracy and computational effort is achieved using lone-ions-SMD calculations. Lone-ions-SMD calculations are the simplest and cheapest model (studied here) that accurately captures the IL DoS. We have shown that lone-ions-SMD matches well to experimental data both qualitatively (visual matches to experimental valence XP spectra and RXP spectra) and quantitatively (linear correlations for E_i(IL) and ΔE_B(ion HOFO)). Using lone-ions-SMD compared to *e.g.*, five ion-pairs (where the effect of the counterions would be close to fully captured) causes minimal loss of output quality with respect to the valence levels, and avoids the necessity of dynamically sampling a wide range of cluster conformers.

Relative to the lone-ions-SMD, calculations involving ion-pairs and dimers carry a significantly greater computational cost and require more skill to generate and evaluate, and thus are too expensive and time-consuming for screening many ILs. An attempt has been made to quantify the computational cost saving for different model systems (ESI,† Table S4). As more ions are added to a system, a larger number of possible conformers (relative arrangement of the cations and anions) needs to be evaluated. Broadly, the time saved increases as more ILs are screened. For example, to screen 1000 ILs made up from a pool of 20 cations and 50 anions, the lone-ions calculations have ∼430 times lower computational cost than ion-pair calculations and ∼7900 times lower computational cost than dimer calculations (ESI,† Table S4). These estimates do not include the user time required to select the ion-pair/dimer conformers or run a dynamic sampling procedure, which is very dependent on the experience of the user.

The additivity of the individual cation and anion lone-ion calculation results provides a significant advantage when screening IL combinations, and means low-cost predictions of DoS can be achieved for a large number of ILs. We have made predictions based on 16 cations and 35 anions, which can form 560 different ILs; E_i(calc.) (Fig. 2a) and ΔE_B(ion HOFO,calc.) (Fig. 2b).

Using the validated lone-ions-SMD method, we predict that: (i) the most readily ionised group of ILs is $[cation]_2[FeCl_4]$ with E_i(calc.) = 4.9 eV (Fig. 2a, predicted IL DoS ESI,† Fig. S15a); (ii) the least readily ionised IL is $[N_{2,2,1,0}][SbF_6]$ with E_i(calc.) = 10.1 eV (Fig. 2a, predicted IL DoS ESI,† Fig. S15c). This second result is consistent with the use of ammonium cations and highly fluorinated anions as supporting electrolytes in electrochemistry.[74,75]

ΔE_B(ion HOFO) (Fig. 2b) can be used to identify the ion HOFO that is the IL HOMO (ESI,† Section S8). For ILs it might reasonably be assumed that the anion provides the IL HOMO (*i.e.*, the anion will be ionised before the cation). However, this assumption is not always true. Using the data collected here, the anion is predicted to be the HOMO for 474 ILs and the cation is predicted to be the HOMO for 86 ILs (ESI,† Fig. S14). Thus, 15% of the ILs studied here are predicted to have a cation-based IL HOMO. This conclusion might seem counter-intuitive; for ~15% of ILs the process $[\text{cation}]^+ \rightarrow [\text{cation}]^{2+} + e^-$ is more favourable than the process $[\text{anion}]^- \rightarrow \text{anion} + e^-$. For example, for $[C_4C_1\text{Im}][SbF_6]$ ΔE_B(ion HOFO,calc.) = −2.8 eV (Fig. 2b) is a remarkably large negative value (predicted IL DoS ESI,† Fig. S15b). We have previously shown that atoms of a high electronegativity (within an anion) increase many of the MO E_B, including the HOMO.[22] Anions containing F show a particularly large effect,[22,76] as clearly evidenced in Fig. 2b. The one anion that is not halide-containing (and particularly has no F) that gives a large E_B(anion HOFO) is $[B(CN)_4]^-$ (tetracyanoborate).

For ILs with ΔE_B(ion HOFO,calc.) ≈ 0 eV, which are represented by the white/very pale colored boxes on Fig. 2b (*e.g.*, $[C_nC_1\text{Im}][NTf_2]$ where n = 2 to 8 and $[NTf_2]^-$ = bis[(trifluoromethane)sulfonyl]imide), it is possible that environmental effects could change the relative ordering of the IL ion HOFOs and ultimately affect the IL properties and reactivity. Such ILs could be expected to be more strongly influenced by the presence of solutes such as ion contaminants or water, H-bonding additives or changing IL organisation at an electrode surface.

Conclusions

We show that lone-ions-SMD calculations can be used with a high level of confidence for the prediction of IL DoS; we have predicted the ionisation energy for 560 ILs. The corollary is that lone-ions-SMD calculations can be used to screen ILs without the need for input from experimental data. We have also shown that lone-ions-SMD provides a good balance of accuracy *versus* time/expertise, offering the potential to make predictions for many ILs with minimal additional computational cost or user input. For example, each calculation for a new lone-cation-SMD can be paired with all the previously calculated lone-anion-SMD results. There is potential to develop a database of results for individual lone-ions-SMD, allowing researchers to make predictions of IL DoS for a vast number of ILs without performing a large number of new calculations. Furthermore, we have recently demonstrated that lone-ions-SMD calculations capture ionic liquid local electronic structure.[77]

It is expected that IL DoS will be strongly linked to reactivity. Consequently, further investigation is needed to determine whether this lone-ion-SMD calculation method, and therefore IL DoS, can be used to predict other IL properties and reactivity.

Data availability

Data for this article, including log files for all calculated structures, are available at University of Reading Research Data Archive, DOI: 10.17864/1947.001412. Analysed data supporting this article have been included as part of the ESI.†

Conflicts of interest

There are no conflicts to declare.

Acknowledgements

K. R. J. L. acknowledges support from an Imperial College London Junior Research Fellowship and a Royal Society University Research Fellowship (URF\R\150353 and URF\R\211005). Thanks to Prof. Peter Licence for helpful discussion.

References

1 I. Fleming, *Molecular Orbitals and Organic Chemical Reactions*, Wiley, Chichester, 2010.
2 K. Fukui, *Angew. Chem., Int. Ed. Engl.*, 1982, **21**, 801–809.
3 R. Hoffmann, *Angew. Chem., Int. Ed. Engl.*, 1982, **21**, 711–724.
4 P. Hapiot and C. Lagrost, *Chem. Rev.*, 2008, **108**, 2238–2264.
5 M. Armand, F. Endres, D. R. MacFarlane, H. Ohno and B. Scrosati, *Nat. Mater.*, 2009, **8**, 621–629.
6 D. R. MacFarlane, N. Tachikawa, M. Forsyth, J. M. Pringle, P. C. Howlett, G. D. Elliott, J. H. Davis, M. Watanabe, P. Simon and C. A. Angell, *Energy Environ. Sci.*, 2014, **7**, 232–250.
7 D. R. MacFarlane, M. Forsyth, P. C. Howlett, M. Kar, S. Passerini, J. M. Pringle, H. Ohno, M. Watanabe, F. Yan, W. J. Zheng, S. G. Zhang and J. Zhang, *Nat. Rev. Mater.*, 2016, **1**, 15005.
8 C. Nese and A. N. Unterreiner, *Phys. Chem. Chem. Phys.*, 2010, **12**, 1698–1708.
9 E. W. Castner, C. J. Margulis, M. Maroncelli and J. F. Wishart, *Annu. Rev. Phys. Chem.*, 2011, **62**, 85–105.
10 X. Q. Sun, H. M. Luo and S. Dai, *Chem. Rev.*, 2012, **112**, 2100–2128.
11 A. Brandt, J. Gräsvik, J. P. Hallett and T. Welton, *Green Chem.*, 2013, **15**, 550–583.
12 Y. F. Hu, Z. C. Liu, C. M. Xu and X. M. Zhang, *Chem. Soc. Rev.*, 2011, **40**, 3802–3823.
13 X. P. Zhang, X. C. Zhang, H. F. Dong, Z. J. Zhao, S. J. Zhang and Y. Huang, *Energy Environ. Sci.*, 2012, **5**, 6668–6681.
14 For calculations in this article, the HOMO refers to the lowest energy valence level in the ground state of the molecule or ion. For experimental XPS in this article, the HOMO refers to the most readily ionised valence level of the molecule or ion. A. Kahn, *Mater. Horiz.*, 2016, **3**, 7–10.
15 V. R. Koch, L. A. Dominey, C. Nanjundiah and M. J. Ondrechen, *J. Electrochem. Soc.*, 1996, **143**, 798–803.
16 P. Ballone and R. Cortes-Huerto, *Faraday Discuss.*, 2012, **154**, 373–389.
17 I. Kuusik, M. Kook, R. Parna and V. Kisand, *ACS Omega*, 2021, **6**, 5255–5265.
18 K. L. Van Aken, M. Beidaghi and Y. Gogotsi, *Angew. Chem., Int. Ed.*, 2015, **54**, 4806–4809.

19 R. G. Pearson, *J. Am. Chem. Soc.*, 1986, **108**, 6109–6114.
20 R. G. Pearson, *Inorg. Chem.*, 1988, **27**, 734–740.
21 R. M. Fogarty, R. G. Palgrave, R. A. Bourne, K. Handrup, I. J. Villar-Garcia, D. J. Payne, P. A. Hunt and K. R. J. Lovelock, *Phys. Chem. Chem. Phys.*, 2019, **21**, 18893–18910.
22 J. M. Seymour, E. Gousseva, A. I. Large, C. J. Clarke, P. Licence, R. M. Fogarty, D. A. Duncan, P. Ferrer, F. Venturini, R. A. Bennett, R. G. Palgrave and K. R. J. Lovelock, *Phys. Chem. Chem. Phys.*, 2021, **23**, 20957–20973.
23 J. M. Kahk, I. Kuusik, V. Kisand, K. R. J. Lovelock and J. Lischner, *npj Comput. Mater.*, 2020, **6**, 148.
24 E. I. Izgorodina, Z. L. Seeger, D. L. A. Scarborough and S. Y. S. Tan, *Chem. Rev.*, 2017, **117**, 6696–6754.
25 D. Yoshimura, T. Yokoyama, T. Nishi, H. Ishii, R. Ozawa, H. Hamaguchi and K. Seki, *J. Electron Spectrosc. Relat. Phenom.*, 2005, **144**, 319–322.
26 T. Nishi, T. Iwahashi, H. Yamane, Y. Ouchi, K. Kanai and K. Seki, *Chem. Phys. Lett.*, 2008, **455**, 213–217.
27 K. Kanai, T. Nishi, T. Iwahashi, Y. Ouchi, K. Seki, Y. Harada and S. Shin, *J. Electron Spectrosc. Relat. Phenom.*, 2009, **174**, 110–115.
28 K. Kanai, T. Nishi, T. Iwahashi, Y. Ouchi, K. Seki, Y. Harada and S. Shin, *J. Chem. Phys.*, 2008, **129**, 224507.
29 T. Iwahashi, T. Nishi, H. Yamane, T. Miyamae, K. Kanai, K. Seki, D. Kim and Y. Ouchi, *J. Phys. Chem. C*, 2009, **113**, 19237–19243.
30 S. Krischok, R. Öttking, W. J. D. Beenken, M. Himmerlich, P. Lorenz, O. Höfft, S. Bahr, V. Kempter and J. A. Schaefer, *Z. Phys. Chem.-Int. J. Res. Phys. Chem. Chem. Phys.*, 2006, **220**, 1407–1416.
31 O. Höfft, S. Bahr, M. Himmerlich, S. Krischok, J. A. Schaefer and V. Kempter, *Langmuir*, 2006, **22**, 7120–7123.
32 S. Krischok, M. Eremtchenko, M. Himmerlich, P. Lorenz, J. Uhlig, A. Neumann, R. Öttking, W. J. D. Beenken, O. Höfft, S. Bahr, V. Kempter and J. A. Schaefer, *J. Phys. Chem. B*, 2007, **111**, 4801–4806.
33 M. Reinmöller, A. Ulbrich, T. Ikari, J. Preiss, O. Höfft, F. Endres, S. Krischok and W. J. D. Beenken, *Phys. Chem. Chem. Phys.*, 2011, **13**, 19526–19533.
34 A. Ulbrich, M. Reinmöller, W. J. D. Beenken and S. Krischok, *ChemPhysChem*, 2012, **13**, 1718–1724.
35 A. Ulbrich, M. Reinmöller, W. J. D. Beenken and S. Krischok, *J. Mol. Liq.*, 2014, **192**, 77–86.
36 S. Krischok, A. Ulbrich, T. Ikari, V. Kempter, M. Marschewski and O. Höfft, *Nucl. Instrum. Methods Phys. Res., Sect. B*, 2014, **340**, 51–57.
37 S. Rangan, J. Viereck and R. A. Bartynski, *J. Phys. Chem. B*, 2020, **124**, 7909–7917.
38 L. Šištík, M. Ončák and P. Slavíček, *Phys. Chem. Chem. Phys.*, 2011, **13**, 11998–12007.
39 I. Kuusik, M. Berholts, J. Kruusma, V. Kisand, A. Tonisoo, E. Lust and E. Nommiste, *RSC Adv.*, 2018, **8**, 30298–30304.
40 I. Kuusik, M. Berholts, J. Kruusma, A. Tonisoo, E. Lust, E. Nommiste and V. Kisand, *RSC Adv.*, 2019, **9**, 33140–33146.
41 T. Kurisaki, D. Tanaka, Y. Inoue, H. Wakita, B. Minofar, S. Fukuda, S. Ishiguro and Y. Umebayashi, *J. Phys. Chem. B*, 2012, **116**, 10870–10875.
42 D. Weingarth, I. Czekaj, Z. F. Fei, A. Foelske-Schmitz, P. J. Dyson, A. Wokaun and R. Kötz, *J. Electrochem. Soc.*, 2012, **159**, H611–H615.
43 K. R. J. Lovelock, I. J. Villar-Garcia, F. Maier, H. P. Steinrück and P. Licence, *Chem. Rev.*, 2010, **110**, 5158–5190.
44 J. J. Yeh and I. Lindau, *At. Data Nucl. Data Tables*, 1985, **32**, 1–155.
45 A. V. Marenich, C. J. Cramer and D. G. Truhlar, *J. Phys. Chem. B*, 2009, **113**, 6378–6396.
46 V. S. Bernales, A. V. Marenich, R. Contreras, C. J. Cramer and D. G. Truhlar, *J. Phys. Chem. B*, 2012, **116**, 9122–9129.
47 E. Gousseva, F. K. T. Tompkins, J. M. Seymour, L. G. Parker, C. J. Clarke, R. G. Palgrave, R. A. Bennett, R. Grau-Crespo and K. R. J. Lovelock, *J. Phys. Chem. B*, 2024, **128**, 5030–5043.
48 A. D. Becke, *Phys. Rev. A*, 1988, **38**, 3098–3100.
49 C. T. Lee, W. T. Yang and R. G. Parr, *Phys. Rev. B: Condens. Matter Mater. Phys.*, 1988, **37**, 785–789.
50 M. J. Frisch, G. W. Trucks, H. B. Schlegel, G. E. Scuseria, M. A. Robb, J. R. Cheeseman, G. Scalmani, V. Barone, B. Mennucci, G. A. Petersson, H. Nakatsuji, M. Caricato, X. Li, H. P. Hratchian, A. F. Izmaylov, J. Bloino, G. Zheng, J. L. Sonnenberg, M. Hada, M. Ehara, K. Toyota, R. Fukuda, J. Hasegawa, M. Ishida, T. Nakajima, Y. Honda, O. Kitao, H. Nakai, T. Vreven, J. J. A. Montgomery, J. E. Peralta, F. Ogliaro, M. Bearpark, J. J. Heyd, E. Brothers, K. N. Kudin, V. N. Staroverov, R. Kobayashi, J. Normand, K. Raghavachari, A. Rendell, J. C. Burant, S. S. Iyengar, J. Tomasi, M. Cossi, N. Rega, J. M. Millam, M. Klene, J. E. Knox, J. B. Cross, V. Bakken, C. Adamo, J. Jaramillo, R. Gomperts, R. E. Stratmann, O. Yazyev, A. J. Austin, R. Cammi, C. Pomelli, J. W. Ochterski, R. L. Martin, K. Morokuma, V. G. Zakrzewski, G. A. Voth, P. Salvador, J. J. Dannenberg, S. Dapprich, A. D. Daniels, Ö. Farkas, J. B. Foresman, J. V. Ortiz, J. Cioslowski and D. J. Fox, *Gaussian 09, Revision D.01 ed.*, Gaussian Inc., Wallingford CT, 2009.
51 M. J. Frisch, G. W. Trucks, H. B. Schlegel, G. E. Scuseria, M. A. Robb, J. R. Cheeseman, G. Scalmani, V. Barone, G. A. Petersson, H. Nakatsuji, X. Li, M. Caricato, A. V. Marenich, J. Bloino, B. G. Janesko, R. Gomperts, B. Mennucci, H. P. Hratchian, J. V. Ortiz, A. F. Izmaylov, J. L. Sonnenberg, D. Williams-Young, F. Ding, F. Lipparini, F. Egidi, J. Goings, B. Peng, A. Petrone, T. Henderson, D. Ranasinghe, V. G. Zakrzewski, J. Gao, N. Rega, G. Zheng, W. Liang, M. Hada, M. Ehara, K. Toyota, R. Fukuda, J. Hasegawa, M. Ishida, T. Nakajima, Y. Honda, O. Kitao, H. Nakai, T. Vreven, K. Throssell, J. J. A. Montgomery, J. E. Peralta, F. Ogliaro, M. J. Bearpark, J. J. Heyd, E. N. Brothers, K. N. Kudin, V. N. Staroverov, T. A. Keith, R. Kobayashi, J. Normand, K. Raghavachari, A. P. Rendell, J. C. Burant, S. S. Iyengar, J. Tomasi, M. Cossi, J. M. Millam, M. Klene, C. Adamo, R. Cammi, J. W. Ochterski, R. L. Martin, K. Morokuma, O. Farkas, J. B. Foresman and D. J. Fox, *Gaussian 16, Revision C.01*, Gaussian, Inc., Wallingford CT, 2016.
52 S. Grimme, S. Ehrlich and L. Goerigk, *J. Comput. Chem.*, 2011, **32**, 1456–1465.
53 A. D. Becke and E. R. Johnson, *J. Chem. Phys.*, 2005, **123**, 154101.
54 A. D. Becke and E. R. Johnson, *J. Chem. Phys.*, 2006, **124**, 014104.

55 S. Grimme, J. Antony, S. Ehrlich and H. Krieg, *J. Chem. Phys.*, 2010, **132**, 154104.
56 A. D. McLean and G. S. Chandler, *J. Chem. Phys.*, 1980, **72**, 5639–5648.
57 R. Krishnan, J. S. Binkley, R. Seeger and J. A. Pople, *J. Chem. Phys.*, 1980, **72**, 650–654.
58 T. Clark, J. Chandrasekhar, G. W. Spitznagel and P. V. Schleyer, *J. Comput. Chem.*, 1983, **4**, 294–301.
59 M. J. Frisch, J. A. Pople and J. S. Binkley, *J. Chem. Phys.*, 1984, **80**, 3265–3269.
60 W. R. Wadt and P. J. Hay, *J. Chem. Phys.*, 1985, **82**, 284–298.
61 R. Rowe, K. R. J. Lovelock and P. A. Hunt, *J. Chem. Phys.*, 2021, **155**, 014501.
62 K. A. Peterson, *J. Chem. Phys.*, 2003, **119**, 11099–11112.
63 K. A. Peterson, D. Figgen, E. Goll, H. Stoll and M. Dolg, *J. Chem. Phys.*, 2003, **119**, 11113–11123.
64 R. Rowe, PhD thesis, Imperial College London, 2019.
65 J. P. Perdew, R. G. Parr, M. Levy and J. L. Balduz, *Phys. Rev. Lett.*, 1982, **49**, 1691–1694.
66 M. Levy, J. P. Perdew and V. Sahni, *Phys. Rev. A*, 1984, **30**, 2745–2748.
67 D. P. Chong, O. V. Gritsenko and E. J. Baerends, *J. Chem. Phys.*, 2002, **116**, 1760–1772.
68 C. G. Zhan, J. A. Nichols and D. A. Dixon, *J. Phys. Chem. A*, 2003, **107**, 4184–4195.
69 G. Zhang and C. B. Musgrave, *J. Phys. Chem. A*, 2007, **111**, 1554–1561.
70 C. Wakai, A. Oleinikova, M. Ott and H. Weingärtner, *J. Phys. Chem. B*, 2005, **109**, 17028–17030.
71 M. M. Huang, Y. P. Jiang, P. Sasisanker, G. W. Driver and H. Weingärtner, *J. Chem. Eng. Data*, 2011, **56**, 1494–1499.
72 H. Weingärtner, *J. Mol. Liq.*, 2014, **192**, 185–190.
73 A. Stoppa, J. Hunger, R. Buchner, G. Hefter, A. Thoman and H. Helm, *J. Phys. Chem. B*, 2008, **112**, 4854–4858.
74 N. Elgrishi, K. J. Rountree, B. D. McCarthy, E. S. Rountree, T. T. Eisenhart and J. L. Dempsey, *J. Chem. Educ.*, 2018, **95**, 197–206.
75 F. Mast, M. M. Hielscher, T. Wirtanen, M. Erichsen, J. Gauss, G. Diezemann and S. R. Waldvogel, *J. Am. Chem. Soc.*, 2024, **146**, 15119–15129.
76 R. P. Matthews, C. Ashworth, T. Welton and P. A. Hunt, *J. Phys.-Condes. Matter*, 2014, **26**, 284112.
77 F. K. Towers Tompkins, L. G. Parker, R. M. Fogarty, J. M. Seymour, R. Rowe, R. G. Palgrave, R. P. Matthews, R. A. Bennett, P. A. Hunt and K. R. J. Lovelock, *Phys. Chem. Chem. Phys.*, 2025, DOI: **10.1039/D5CP00892A**.